Pergamon

Adv. Space Res. Vol. 18, No. 8, pp. (8)171–(8)186, 1996

0273-1177/96 $9.50 + 0.00

0273-1177(95)00969-8

NEW HIGH TEMPORAL AND SPATIAL RESOLUTION MEASUREMENTS BY SAMPEX OF THE PRECIPITATION OF RELATIVISTIC ELECTRONS

J. B. Blake,* M. D. Looper,* D. N. Baker,** R. Nakamura,***
B. Klecker† and D. Hovestadt†

* *The Aerospace Corporation, Los Angeles, CA 90009, U.S.A.*
** *LASP, University of Colorado, Boulder, CO 80309, U.S.A.*
*** *Solar-Terrestrial Environment Laboratory, Nagoya University, Toyokawa 442, Japan*
† *MPI für Extraterrestrische Physik, Garching bei München, Germany*

ABSTRACT

The precipitation of electrons of 150 keV and 1 MeV in the outer zone have been measured by an instrument aboard the low-altitude, polar-orbiting SAMPEX (Solar, Anomalous, and Magnetospheric Particle Explorer)satellite. This instrument has an extremely large geometric factor (100 cm^2 sr at 1 MeV) and is sampled ten times per second. Broad areas of strong precipitation, extending ~ 2–3° in latitude, frequently are observed near the high-latitude boundary of the outer zone. These features can persist for hours and are seen in conjugate locations. A transient form of strong precipitation, a microburst, is also seen regularly. Microbursts often are seen lasting for less than a second, indicating that microbursts sometimes occur in a very localized region; the narrow temporal structure is a consequence of the orbital velocity of SAMPEX. In other cases, where the spatial size is greater, the temporal evolution of the microburst can be followed. These sum of these observations clearly indicates that outer-zone electron precipitation frequently results from a strong scattering process, and not by weak diffusion of stably trapped electrons into the drift loss cone.

INTRODUCTION

The precipitation of energetic electrons (energies of a few hundred keV and above) was one of the first areas of exploration in the Earth's magnetosphere /1–6/. Studies continued, governed as always by flight opportunities, until the present day /7–15/. This research has shown energetic electron precipitation to be continuous at some level, highly complex and dynamic, and the major sink for magnetospheric electrons.

The great temporal variability in the observed electron fluxes, caused both by actual transitory changes and by the rapid motion of a low-altitude satellite through differing magnetospheric regions, has been one of the major difficulties in gaining an understanding of the underlying physics. One obvious approach in dealing with this problem is to increase the sampling rate of the spacecraft instrumentation. However, this will lead to statistical problems unless there is a corresponding increase in the geometric factor of the sensor. The SAMPEX (Solar, Anomalous, and Magnetospheric Particle Explorer) mission contains instrumentation that combines high-rate sampling of the data with a very large geometric factor, giving a new opportunity to study the precipitation of energetic electrons. In this paper, we briefly describe the HILT (Heavy Ion Large Telescope) sensor and show some typical observations and analysis. The focus is on the magnetospheric locations and temporal fluctuations of the electron precipitation. Local time and magnetic activity dependencies will be deferred to a later publication.

SATELLITE AND INSTRUMENTATION

SAMPEX was launched into a 520 × 670-km altitude, 82° inclination Earth orbit on 3 July 1992 /16/. Its complement of four energetic-particle instruments included HILT /17/, the primary purpose of which is to measure elemental abundances, energy spectra, and direction of incidence for ions from helium to iron in the energy range of 4 to 250 MeV/nucleon. In addition, HILT provides very high-sensitivity and time-resolution measurements of electrons with energies > 150 keV and 1 MeV.

Figure 1 shows a cross-section of the HILT sensor and its mounting configuration on the SAMPEX satellite. Sixteen solid-state SiLi detectors are placed in a square array at the back of the HILT sensor; in front of this array is an ion chamber and two proportional counters (PCs) filled with 75 Torr of isobutane. The lower-energy electron measurements discussed in this paper use the rear PC, which is placed directly in front of the solid-state detectors (SSDs). The silicon detectors each have an area of 10 cm^2 and a thickness of 2 mm. These 16 detectors are grouped into four rows of four detectors; each row is connected to a separate preamplifier-amplifier chain with a discriminator threshold of 1 MeV. The count rate in each row of detectors is sampled 10 times per second. The rear PC is a single very large detector; it also is sampled 10 times per second.

Zenith pointing of the sensor complement is routinely maintained at high latitudes. The magnetic-field vector is shown in Figure 1, making an angle, θ, with the zenith. In the outer zone and poleward, the region of interest in this paper, θ is of the order of 30° or less. For the relative positioning of the zenith and the magnetic field as shown, detector Row 1 "sees" closer to the mirror plane over the edge of the HILT aperture than do the other three rows. Row 4 has the poorest view. As a result, if the loss cone is empty, the count rate will be highest in Row 1 and lowest in Row 4. Rows 2 and 3 will have count rates intermediate between Rows 1 and 4. On the other side of the polar cap, where the magnetic field makes an angle of $-\theta$ with the zenith, the viewing situation reverses. Row 4 views closest to the mirror plane and will have the highest count rate. When the loss cone is filled, the electrons are isotropic over the HILT aperture, and, as a result, all four detector rows show the same count rate. In principle, the relative count rates of the four rows could be used to determine the pitch-angle distribution. However, in practice, scattering in the HILT entrance windows, in the isobutane gas, and on the chamber walls smears the angular measurements and makes such estimates uncertain. In this paper, we use the relative SSD count rates only to determine if the loss cone is filled.

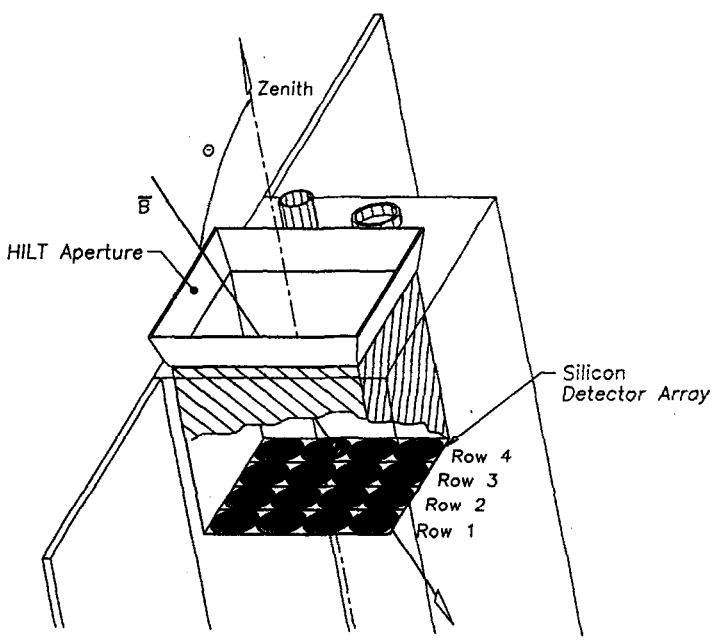

Fig. 1. Cross-section of the HILT instrument as mounted on the SAMPEX satellite. The square array of 16 SSDs is shown with the four rows explicitly shown.

Figure 2 presents the results of Monte Carlo calculations of the efficiencies/geometric factors of the SSDs and the rear PC as a function of incident electron energy. The results for the SSDs are for the sum of all four detector rows; for an isotropic flux, each row responds identically. The PC plot shows the result calculated for discriminator thresholds of 15 keV and 30 keV. The threshold at launch was 15 keV. However, with time, the threshold increased by about a factor of 2; the actual value is readily determined by examining the response of HILT to cosmic-ray ions. The decrease in effective PC threshold is believed to be due to the collection of isobutane fragments on the anode wires of the PC. In the following text, we refer to 1-MeV and 150-keV electrons as a shorthand way to describe the actual response function shown in Figure 2.

OBSERVATIONS

Figure 3 shows the count rate per 100 ms of the four rows of SSDs, each row plotted in a different color, over a 400-s interval on Day 92278 as SAMPEX moved to high latitude through the outer zone and out over the polar cap. The count rate of the PC is shown in black; the PC is in saturation much of the time because of the intense electron flux. Near the high-latitude boundary of the outer zone, the count rates of all detectors abruptly increase, and all SSDs show the same count rate, indicating isotropy in the electron fluxes. Prior to that time, the differing count rates in the SSDs are indicative of an unfilled loss cone. We refer to broad regions of precipitation of the type shown in Figure 3 as a precipitation band. The count rates observed over the polar cap result from the low background due to galactic cosmic rays. The lower panel in Figure 3 shows the precipitation band and its immediate vicinity on an expanded scale. Note that the low-latitude edge of the band is at the same location for both 150-keV electrons and 1-MeV electrons, whereas the high-latitude edges differ in location. The precipitation band is approximately twice as wide at 150 keV.

A precipitation band is a common feature near, at, or above the high-latitude boundary of the outer zone as delineated by energetic electrons. Precipitation bands were reported by Anderson et al., /7/ McCoy, /8/ and Brown and Stone /9/ based upon measurements made with instruments aboard the POGO spacecraft. They found that these features occurred below, at, and above the high-latitude boundary of the outer zone and sometimes persisted for hours at the higher latitudes. The earlier work referred to these features as "spikes." We prefer the term "bands" because, as is shown below, much more abruptly varying (spiky) precipitation often is seen. In the SAMPEX data, isotropy is always seen in the precipitation bands, and they are frequently observed to be multiple. When multiple, the precipitation bands show more structure within each band.

Figure 4 shows observations of multiple bands made on Day 93079; the lower panel shows the first two precipitation bands at a higher time resolution. SAMPEX was moving equatorward during the time interval shown. (Note that the relative count rates of the four SSD rows at lower latitudes in Figure 4 are the reverse of that for the case shown in Figure 3; SSD 1 > SSD 2 > SSD 3 > SSD 4 rather than the reverse, showing explicitly the sensitivity of HILT to the angular distributions of the electrons.) The highly irregular character of the precipitation, as well as the different spectral hardness of the electron precipitation from one band to the next, can be seen clearly. (Only a qualitative estimate of the energy spectrum can be made using the two HILT energy channels.) The first very narrow band, at the highest latitude, is spectrally harder than the second; in fact the 1-MeV rate is larger than the 150-keV rate in the first band. Figure 4 shows that the subsequent four bands have a variety of characteristics differing in spectral hardness, latitudinal width, and amount of variability within a given band. An interesting difference between the precipitation band shown in Figure 3 and the multiple bands shown in Figure 4 is that the widths of the multiple bands are the same at 150 keV and 1 MeV, unlike the case for the single band. This frequently seems to be a characteristic difference between single and multiple bands in the SAMPEX data. Because single bands often are located on the outer zone boundary, this characteristic may result from the energy dependence of the boundary of durable trapping /11,15/.

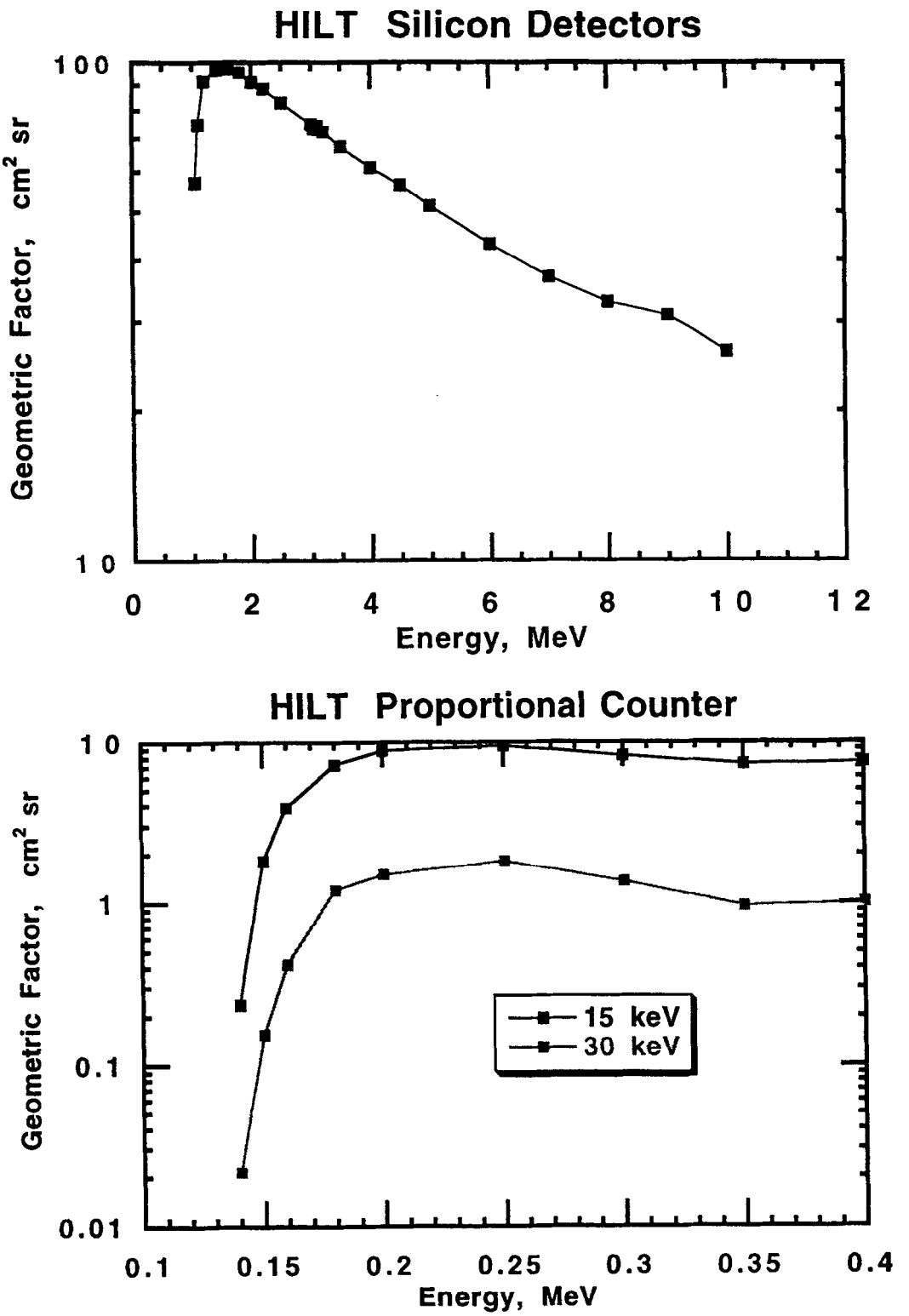

Fig. 2. Efficiencies/geometric factors as a function of incident electron energy of the HILT silicon detectors and rear proportional counter. Calculations were carried out using a Monte Carlo radiation-transport code; an isotropic incident flux was assumed.

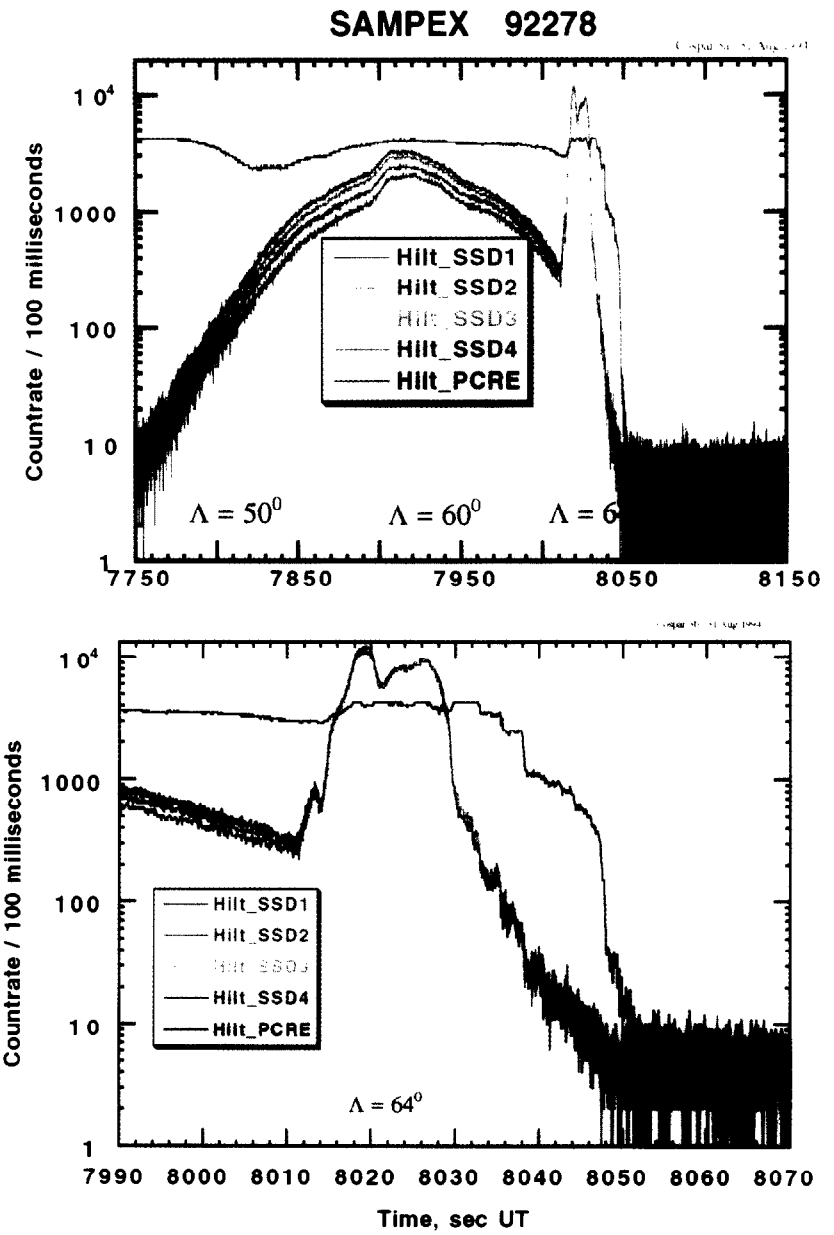

Fig. 3. Count rates of the four SSDs and the rear PC plotted as a function of time for an outer-zone traverse early on Day 92278. The upper panel shows the entire pass from below an invariant latitude of 50° until SAMPEX was over the polar cap. The lower panel is an expanded view of the time period when the large precipitation band was observed; the band was located at an invariant latitude of around 64°.

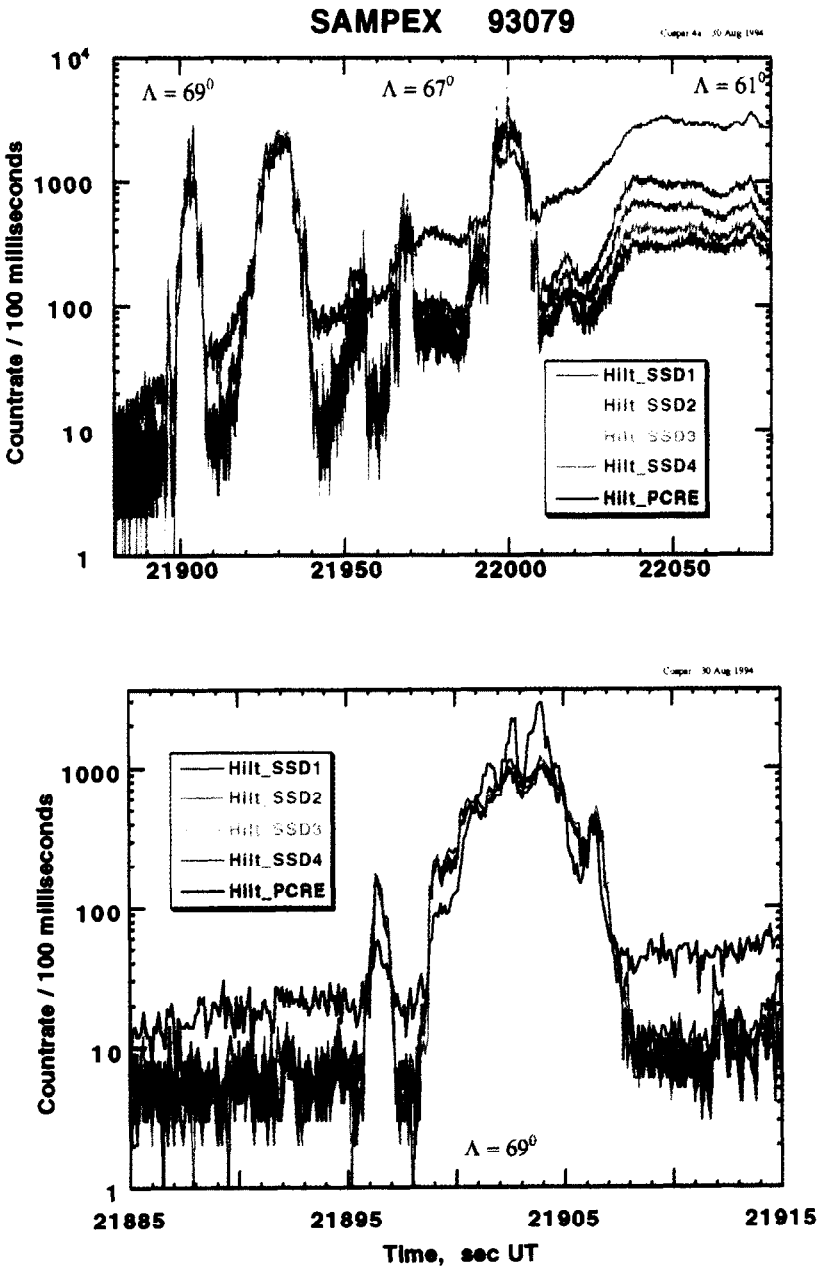

Fig. 4. Count rates of the five HILT channels for an outer zone pass on Day 93079 showing an example of multiple precipitation bands. The bottom panel shows the first two bands encountered (at the highest latitude) on an expanded scale. The second band can be seen to have been observed at an invariant latitude of 69°.

Figure 5 shows another very common type of energetic-electron precipitation seen in the SAMPEX data, characterized by intense bursts and often appearing clustered in groups. Because of their short, highly irregular structure, we refer to them as microbursts /18/. The term microburst was coined by Anderson and Milton /19/ to describe auroral-zone balloon observations of bremsstrahlung bursts at energies > 30 keV. Microbursts in the SAMPEX data are seen near the trapping boundary, but definitely are not confined to that region; they routinely are observed at substantially lower latitude well away from the auroral zone. The time-expanded plot, lower panel, shows that the microbursts often have an abrupt rise and a substantially slower decay, and the loss cone fills in some of the larger microbursts. Throughout the time period shown in the lower panel, the PC was in hard saturation due to the high electron fluxes; therefore, details of the > 150-keV electron precipitation cannot be discerned.

Figure 6 shows the intense microburst that occurred just after 14310 s UT on Day 92278, Figure 5, on a greatly expanded timescale; this plot covers only eight seconds. The lower panel shows all four SSD channels as in the earlier plots; the upper panel is a plot of only SSD Row 1, with error bars given for each 100-ms sample. Prior to the microburst onset, the markedly different rates in the four detector rows indicate an empty loss cone. Then, within a few hundred milliseconds, the count rates greatly increase and become identical. Subsequently, the microburst dies away over a few seconds in a sawtooth fashion. Apparently a burst of electron scattering occurred at high altitude, which filled the loss cone. The scattering event was short relative to the electron bounce period; as a result, the loss cone was not filled all along the flux tube. A packet of electrons had been created that bounced from mirror point to mirror point, losing a substantial fraction of the loss-cone flux in the atmosphere at each bounce. HILT observed the bouncing packet, which decreased in intensity at succeeding observations. The sawtooth structure was created by the finite width of the packet along the field line; the packet was not always present at SAMPEX during the time of a data sample. If the backscatter fraction were 1/e (a fair approximation) then the microburst would decay with an e-folding time of half a bounce period. The HILT sample rate was a few times the bounce period, enabling the phenomena to be clearly delineated.

Another example of highly structured precipitation is shown in Figure 7. The flux in the microbursts increased by more than 3 orders of magnitude in the largest microbursts. Here also, the PC was saturated much of the time, although not driven to hard saturation as was the case for the events shown in Figure 5. SAMPEX, during the time interval shown in Figure 7, was over the Western North Atlantic. As a consequence, during the first half of the plotted time period, the conjugate mirror point was below sea level, which can account for the fact that the trapped flux measured between the microbursts was nil. The expanded plot in the lower panel shows that the microbursts were narrow, at times less than a second in width. Microbursts of the character exemplified by those shown in Figure 5 do not appear.

DISCUSSION

Precipitation Bands.

As noted above, what we have termed precipitation bands were discovered over 20 years ago /7,8,9/. The characteristics of the HILT sensor have enabled us to add to these earlier studies, in particular, to determine that within the precipitation bands, the loss cone is filled. Strong precipitation is occurring whenever these features are encountered. If precipitation occurred West of the satellite and had ceased at the location of SAMPEX, those electrons in the bounce loss cone would have been lost into the atmosphere by the time SAMPEX was encountered. In such an event, the precipitation band would be observed with a trapped distribution. This is not seen in these events, and this situation is especially clear in the case of single precipitation bands exemplified by Figure 3. This characteristic strongly suggests that the band precipitation takes place over an extended region in longitude and that the repeated encounters with very similar structures orbit after orbit indicates that the precipitation can continue for hours /18/. In fact, the SAMPEX data show that precipitation bands can persist for over half a day, remaining at the same invariant latitude and appearing at conjugate locations. Brown and Stone /9/ reported similar observations for > 425-keV electrons.

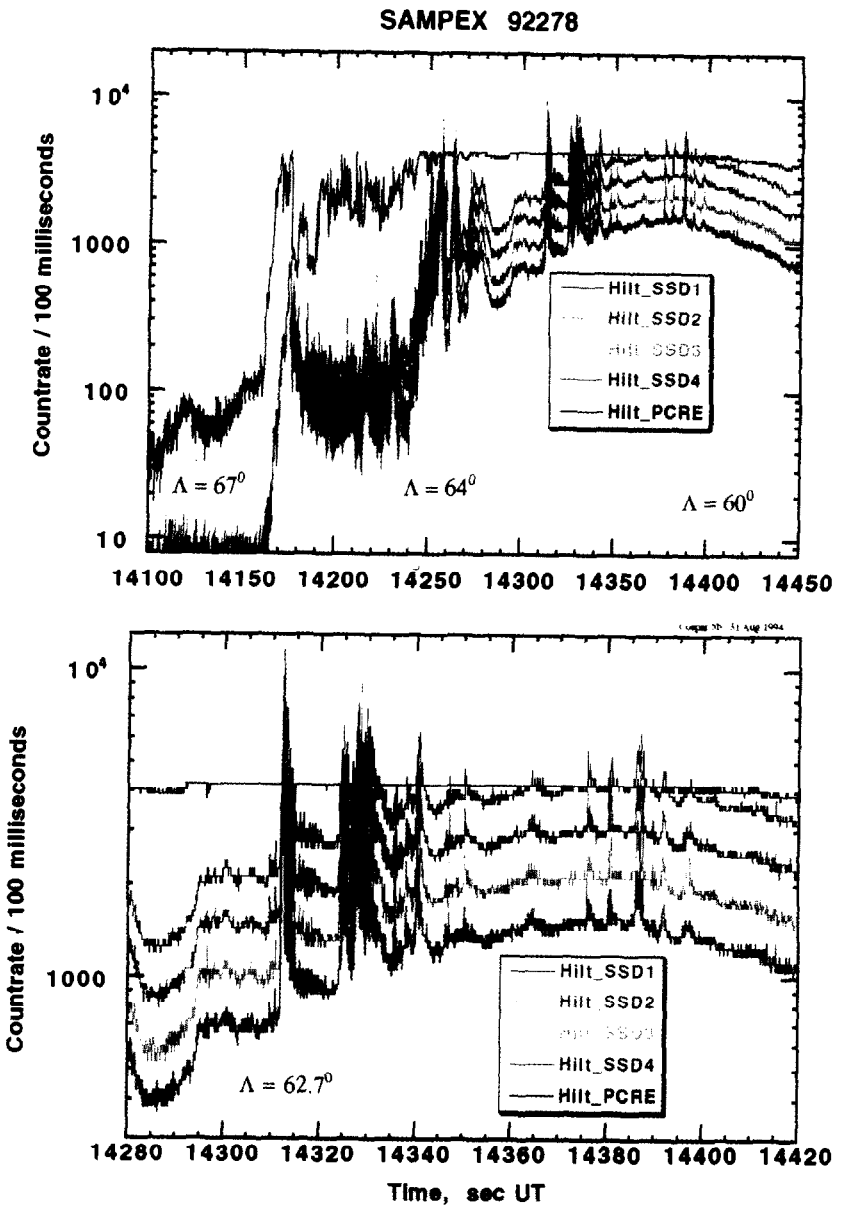

Fig. 5. The high-latitude portion of an outer zone pass is shown for the five HILT channels on Day 92278. This pass shows many examples of microbursts. A portion of the pass is shown on an expanded scale in the bottom panel.

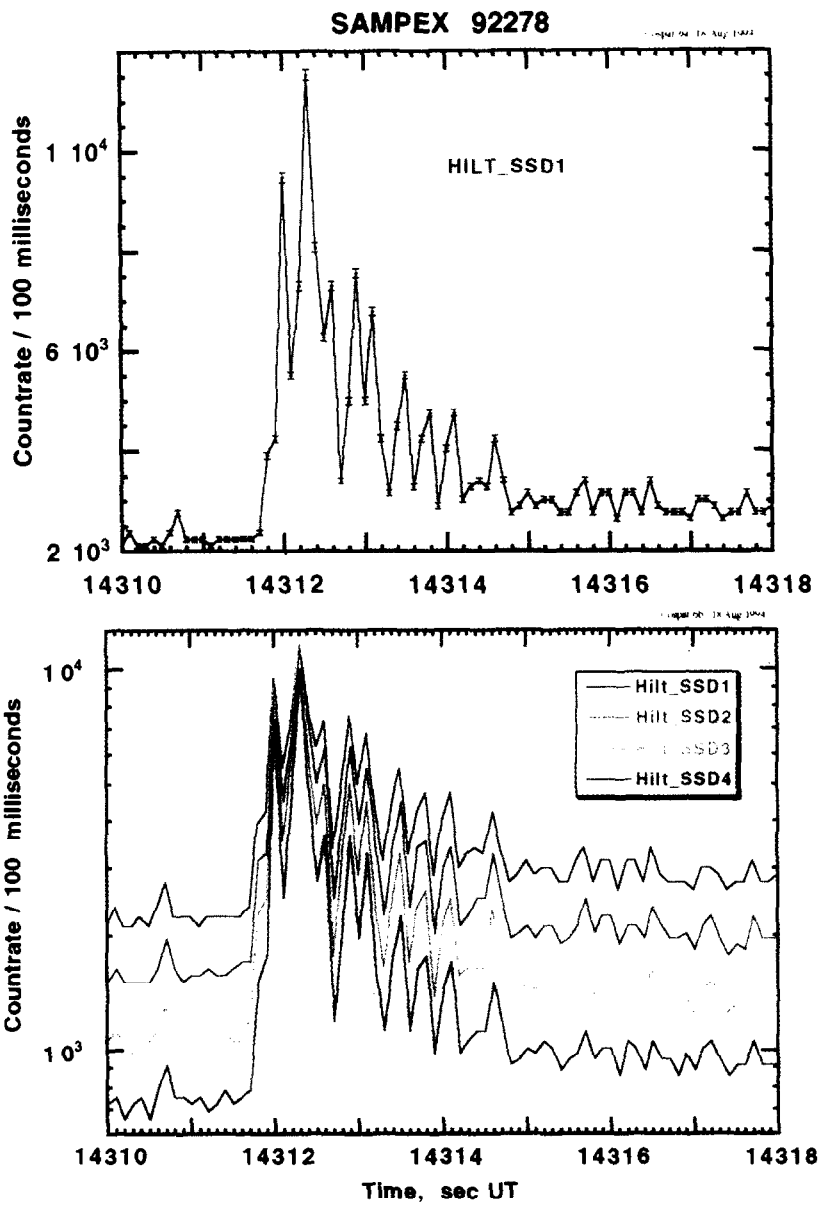

Fig. 6. Portion of the outer zone pass shown in Figure 5 shown on a greatly expanded scale. The entire figure covers only 8 s. The bottom panel presenting all four SSD count rates clearly shows the abrupt transition to isotropy at the start of the microburst at 14312 UT, followed by a sawtooth decay back to a condition of anisotropic fluxes. The top panel shows only one channel with the error bars plotted on each data point, showing that the statistical errors are nil.

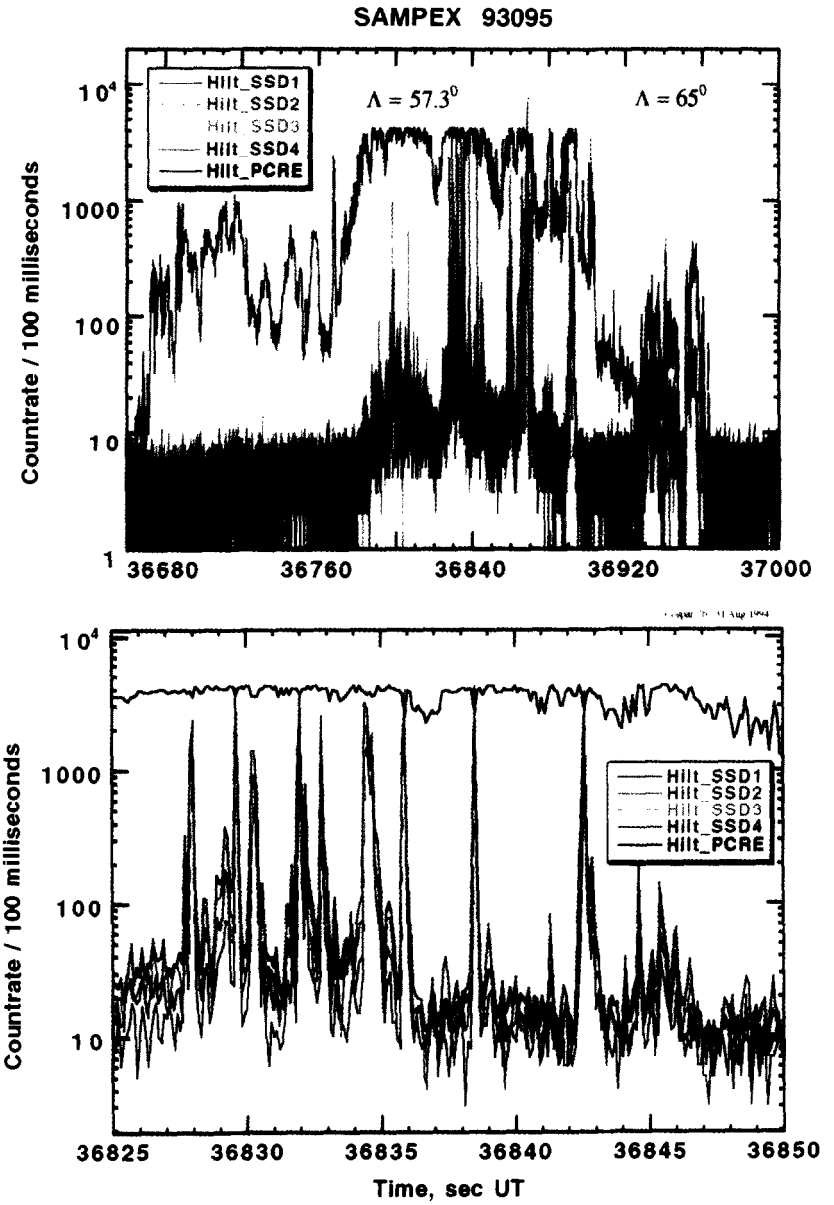

Fig. 7. Count rates of the five channels shown for an outer-zone pass on Day 93095. During this pass, SAMPEX was over the eastern part of the North Atlantic where, for much of the pass, the conjugate mirror point of the electrons was below sea level. The bottom panel shows many microbursts less than 1 s wide.

The precipitation bands frequently contain the most intense flux encountered throughout a SAMPEX outer-zone pass, cf. Figure 3. Strong pitch-angle scattering at high altitude results in SAMPEX sampling the high-altitude flux and not the stably trapped flux present at low altitude. An extreme example, observed on Day 93079, is shown in Figure 8. The locally trapped flux at 1 MeV throughout the pass was nil. Only a precipitation band appears, and within this band, the SSDs were driven to saturation. The precipitation energy within the band was at least 0.5 ergs/cm^2-s above 1 MeV. (We have assumed, in order to make this estimate, that all electrons were 1 MeV and corrected for deadtime in the SSD count rates.)

Microbursts

The cyclotron radius of the electrons, their bounce and drift speeds, and the motion of SAMPEX are all factors that set limits on what precipitation characteristics can be observed by SAMPEX. In Figure 9, the top panel gives the average electron gyroradius as a function of electron energy at the SAMPEX altitude and the residence time of SAMPEX within one electron gyroradius. Since the HILT sampling period is 100 ms, SAMPEX moves of the order of two gyroradii per sample. The middle panel *(??)* displays the bounce period of 1-MeV electrons as a function of L value and the latitudinal distance that SAMPEX moves per electron bounce. In order to be able to observe the evolution of a bouncing electron packet, such as shown in Figure 6, the latitudinal size of the precipitation region must be at least a few tens of kilometers. The bottom panel shows the drift period of 1-MeV electrons as a function of L value and the resulting longitudinal distance that an electron moves per bounce. Note that this distance is of the order of three times the latitudinal distance SAMPEX moves per bounce. Furthermore, SAMPEX moves North or South, whereas the electrons drift East; a dimensionally small electron packet could leapfrog SAMPEX.

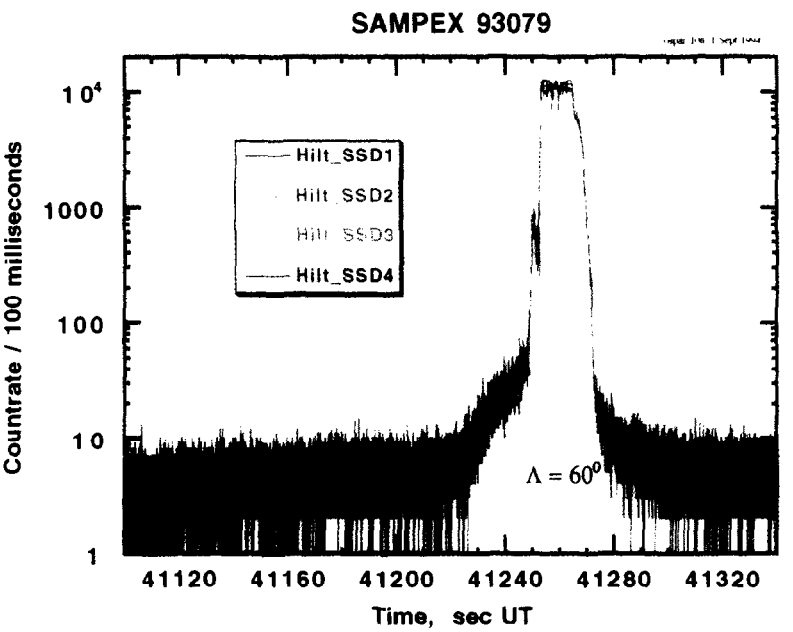

Fig. 8. Intense precipitation band observed on Day 93079 when the local trapped flux was at an almost non-existent level.

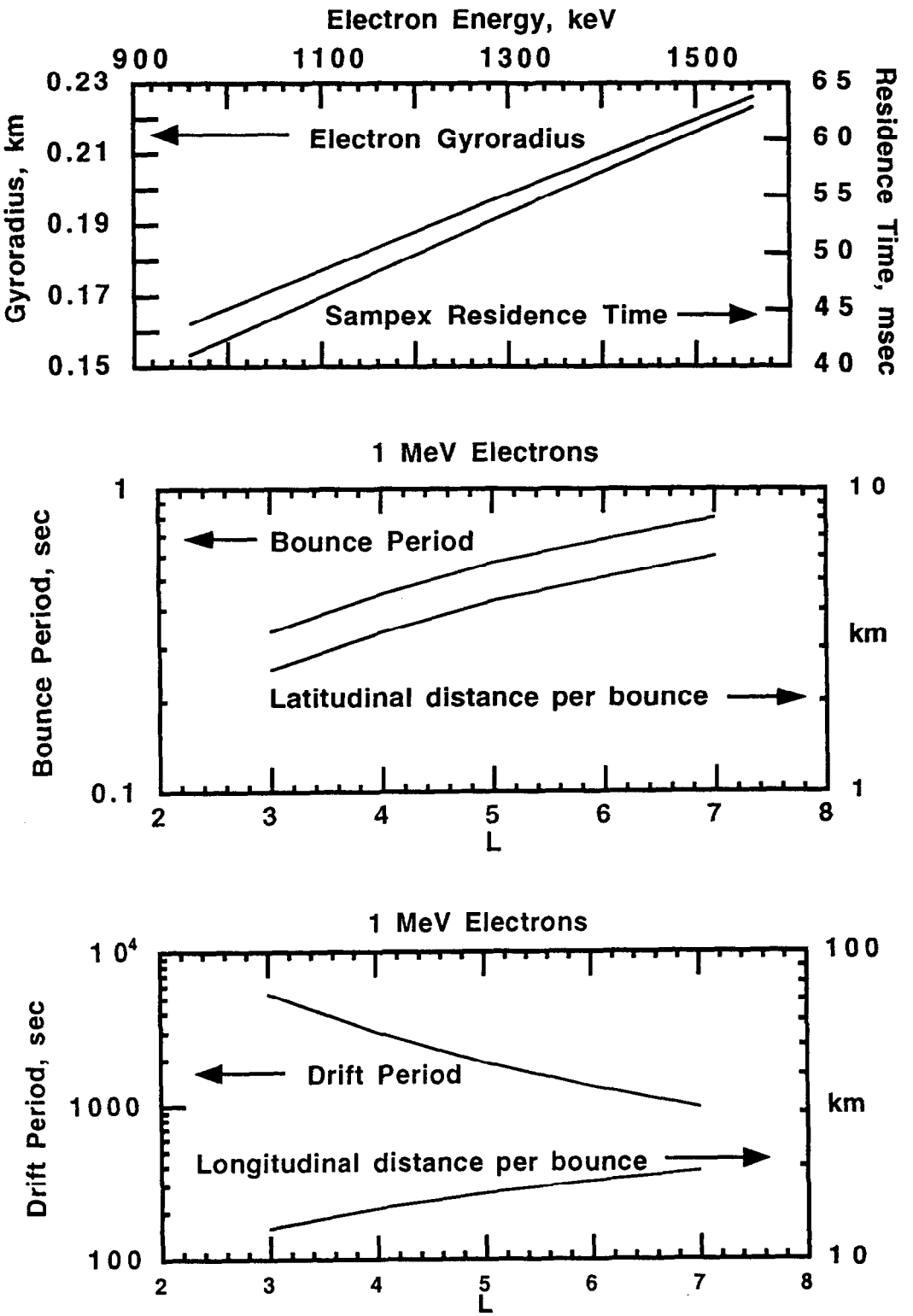

Fig. 9. Top panel: electron gyroradius and residence time of SAMPEX within a gyroradius plotted as a function of electron energy. Middle panel: plot of the bounce period of 1-MeV electrons as a function of L value (small equatorial pitch angle) and the latitudinal distance SAMPEX moves in one electron bounce period. Lower panel: plot of the drift period of 1-MeV electrons as a function of L value and the longitudinal distance the electrons move per bounce period.

The key point is that a relativistic electron microburst with a scale size of less than several tens of gyroradii cannot be observed completely by SAMPEX. A perusal of many days of SAMPEX data shows relatively few examples of a microburst such as shown in Figure 6, where the onset and entire decay was witnessed. Extremely common are observations such as shown in Figure 7, where a "forest" of narrow spikes are seen. Obviously, atmospheric losses cannot cause such a rapid decay of the electron intensity. At each interaction with the atmosphere, the backscatter is a few tens of percent; the decay can be no faster. Therefore, we interpret the very commonplace observations exemplified by Figure 7 as demonstrating the fact that microbursts, in general, have a scale size of a less than a few tens of electron gyroradii. In the future, a statistical analysis of microburst widths should enable us to make an estimate of their mean size.

The combination of electron-energy spectra, geometric factors, and efficiencies in general lead to the situation that if the SSD counting rates are sufficiently large for good statistical sampling, the PC is saturated. However, by careful selection of time periods, one can find cases where the temporal structure of the 150-keV and 1-MeV microbursts can be directly compared. Figure 10 shows two such examples taken from portions of the data shown in Figures 5 and 7. The top panel (Day 92278) shows that the microburst structures at 150 keV and 1 MeV are not always well correlated; there clearly is a strong electron-energy dependence in the precipitation process. The bottom panel in (Day 93095) shows that the microbursts at 150 keV can be as narrow as those at 1 MeV. However, as exemplified by the data shown in Figure 7, the latitudinal width of a precipitation region at 150 keV usually is substantially broader than at 1 MeV. In addition, at 150 keV, the microbursts appear to coalesce into broader regions of precipitation. In the run of data shown in Figure 7, the 1-MeV plot has a pin-cushion appearance, whereas the 150-keV data shows broad enhancements with embedded high-frequency structure.

Following the precipitation microburst shown in Figure 6, additional microbursts occurred, cf. Figure 5. In most cases, the loss cone was not filled, although the ratios of SSD count rates become more equal, suggesting filling of the drift loss cone. These microbursts are interpreted as being much like the one shown in Figure 6, but with the scattering event occurring to the West of SAMPEX. The electrons in the bounce loss cone have been removed; however, electrons scattered into the drift loss cone remain and are seen as an increase in local electron fluence. Note that the larger of such microbursts show the rapid rise and slower fall of the event displayed in Figure 6, whereas the smaller microbursts are more smeared. This observation is consist with the smaller microbursts resulting from scattering events occurring substantially further to the West of SAMPEX and, as a result, becoming much more smeared by the energy-dependent drift speeds of the electrons above the HILT threshold.

The region between microbursts is also of interest. Following the single microburst depicted in Figure 6, the electron flux can be seen to vary in an irregular way. The small size of the error bars shows that the varying intensity is not due to statistical fluctuations but result from an actual change in electron flux. We interpret these variations of electron fluxes as a summing of microbursts that occurred well to the West of SAMPEX and have become smeared out and intermixed over many degrees of longitudinal drift. Many studies have found energetic electrons to be in the drift loss cone at times, but in regions where the bounce loss cone is empty. One interpretation for such observations is that wave-particle interactions have scattered the electrons only a small amount, moving those electrons with pitch angles very near to but not in the drift loss cone over the edge of the stable trapping region in pitch-angle space and into the drift loss cone. These SAMPEX observations indicate that frequently another process is taking place. Microbursts of electron scattering occur that fill both the drift loss cone and the bounce loss cone. Those electrons in the bounce loss cone are quickly lost, leaving to be seen only those in the drift loss cone. The very large geometric factor of the HILT sensor enables us to see that the scattering process often is not spatially broad and weak, but irregular, localized, and strong.

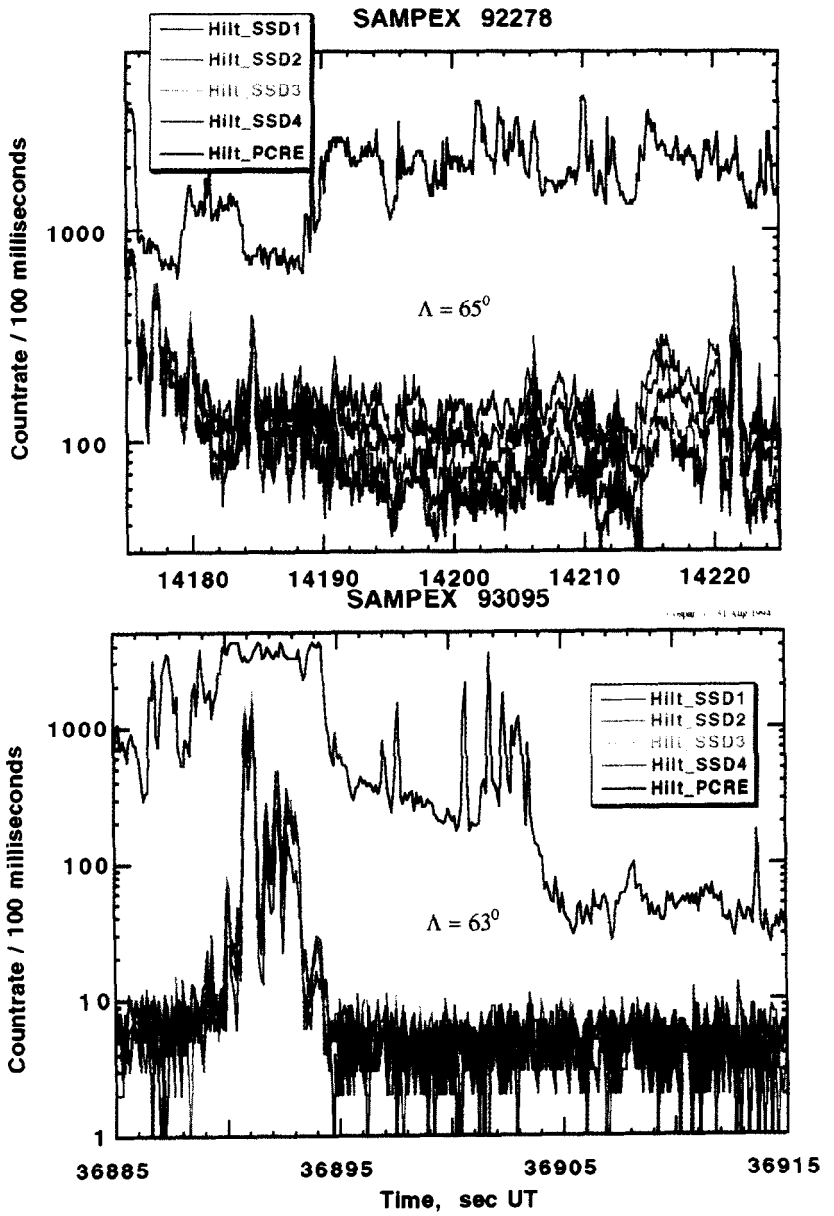

Fig. 10. Five HILT count rates for an outer-zone pass. Top panel: Day 92278; lower panel Day 93095 The data were selected to show comparisons of the temporal structure at 150 keV and 1 MeV.

Imhof et al. /3/ reported satellite observations of relativistic microbursts. They studied the location of the microbursts and found a concentration at the outer edge of the outer zone. These observations led them to conclude that irregularities in the magnetic field, a failure to support adiabatic motion, could be the responsible mechanism for microbursts. As noted above, the SAMPEX observations show microbursts near the trapping boundary as well, but also show microbursts at significantly lower latitude where the magnetic-field configuration almost certainly supports adiabatic motion. A breakdown in adiabatic motion of the relativistic electrons cannot be the single cause of the relativistic microbursts. As illustrated in Figure 5, near the outer zone boundary, microbursts are found immersed in a region of spatially diffuse precipitation. We suspect that two loss processes are operating in this region, one leading to the more or less continuous diffuse precipitation and the other causing microbursts. The diffuse precipitation is more likely an indication of the breakdown of adiabatic motion, with the microbursts resulting from wave-particle interactions. Although microbursts could result from more than one process, Ockham's Razor makes such an assumption unattractive, given presently available evidence.

Figure 5 shows another characteristic of microbursts seen in the SAMPEX data; the microbursts tend to appear in trains of pulses or associated groups. It appears that near the equator, where presumably the electron scattering is occurring, the electron distribution is marginally stable over a rather broad region. Strong scattering begins abruptly in a small part of this region and is quickly damped. Anderson and Milton /19/ reported in their discovery paper the tendency of microbursts to appear grouped into trains of pulses. Their balloon observation platform had an important difference from SAMPEX; they viewed a localized region for an extended period, whereas SAMPEX does not. The balloon observations could have been witness to a relaxation-oscillator process in a localized region of flux tubes, whereas a temporal grouping of microbursts seen by SAMPEX must involve coherence over a more extended region.

ACKNOWLEDGMENTS

This work was supported at The Aerospace Corporation under NASA Cooperative Agreement 26979B, and at the University of Colorado by NAG5-2635.

REFERENCES

1. S. E., Forbush G. Pizzella, and D. Venkatesan, The morphology and temporal variations of the Van Allen radiation belt, October 1959 to December 1960, *J. Geophys. Res.* 67, 3651 (1962).

2. G. A. Paulikas and S. C. Freden, Precipitation of energetic electrons at middle latitudes, *J. Geophys. Res.* 69, 1239 (1964).

3. W. L. Imhof, H. D. Voss, J. Mobilia, D. W. Datlowe, E. E. Gaines, J. P. McGlennon, and U. S. Inan, Relativistic electron microbursts, *J. Geophys. Res.* 97, 13,829 (1992).

4. J. B. Blake, S. C. Freden, and G. A. Paulikas, Precipitation of 400 keV electrons in the auroral zone, *J. Geophys. Res.*, 71, 5129 (1966).

5. G. A. Paulikas, J. B. Blake, and S. C. Freden, Precipitation of energetic electrons at middle latitudes, *J. Geophys. Res.* 71, 3165 (1966).

6. A. J. Zmuda, Ionization enhancement from Van Allen electrons in the South Atlantic magnetic anomaly, *J. Geophys. Res.* 71, 1911 (1966).

7. H. R. Anderson, P. D. Hudson, and J. E. McCoy, Observations of POGO ion chamber experiment in the outer radiation zone, *J. Geophys. Res.* 73, 6285 (1968).

8. J. E. McCoy, High-latitude ionization spikes observed by the POGO ion chamber experiment, *J. Geophys. Res.* 74, 2309 (1969).

9. J. W. Brown and E. C. Stone, High-energy electron spikes at high latitudes, *J. Geophys. Res.* 77, 3384 (1972).

10. A. L. Vampola, H. C. Koons, and D. A. Mcpherson, Outer-zone electron precipitation, *J. Geophys. Res.* 76, 7609 (1971).

11. W. L. Imhof, J. B. Reagan, and E. E. Gaines, Fine-scale spatial structure in the pitch angle distributions of energetic particles near the midnight trapping boundary, *J. Geophys. Res.* 82, 5215 (1977).

12. W. L. Imhof and R. V. Smith, Longitudinal variations of high energy electrons at low altitudes, *J. Geophys. Res.* 70, 569 (1965).

13. W. L. Imhof, H. D. Voss, J. B. Reagan, D. W. Datlowe, E. E. Gaines, J. Mobilia, and D. S. Evans, Relativistic electron and energetic ion precipitation spikes near the plasmapause, *J. Geophys. Res.* 91, 3077 (1986).

14. W. L. Imhof, Fine resolution measurements of the L-dependent energy threshold for isotropy at the trapping boundary, *J. Geophys. Res.* 93, 9743 (1988).

15. W. L. Imhof, H. D. Voss, J. Mobilia, D. W. Datlowe, and E. E. Gaines, The precipitation of relativistic electrons near the trapping boundary, *J. Geophys. Res.* 96, 5619 (1991).

16. D. N. Baker, G. M. Mason, O. Figueroa, G. Colon, J. G. Watzin, and R. M. Aleman, An overview of the Solar, Anomalous, and Magnetospheric Particle Explorer (SAMPEX) mission, *IEEE Trans. Geosciences and Remote Sensing*, 31, 531 (1993).

17 B. Klecker, D. Hovestadt, M. Scholer, H. Arbinger, M. Ertl, H. Kastle, E. Kunneth, P. Laeverenz, E. Seidenschwang, J. B. Blake, N. Katz, and D. Mabry, HILT: A Heavy Ion Large area proportional counter Telescope for solar and anomalous cosmic rays, *IEEE Trans. Geosciences and Remote Sensing*, 31, 542 (1993).

18. R. Nakamura, D. N. Baker, J. B. Blake, S. Kanekal, B. Klecker, and D. Hovestadt, Relativistic electron precipitation near the outer edge of the radiation belt, *Geophys. Res. Lett.*, submitted (1994).

19. K. A. Anderson and D. W. Milton, Balloon Observations of X-Rays in the Auroral Zone, 3. High Time Resolution Studies, *J. Geophys. Res.*, 69, 4457 (1964).